Predicted bound states and microwave spectrum of N_2–He van der Waals complexes

Hui Li,[a] Robert J. Le Roy, and Frederick R. W. McCourt
Department of Chemistry, University of Waterloo, Waterloo, Ontario N2L 3G1, Canada

(Received 31 March 2009; accepted 1 June 2009; published online 26 June 2009)

Numerical calculations show that four modern potential energy surfaces for N_2–He all support 18 bound intermolecular states for the homonuclear isotopologues $^{14,14}N_2$–^{4}He and $^{15,15}N_2$–^{4}He, and 12 (or 13, for one surface) truly bound states for $^{14,15}N_2$–He. This contradicts a recent statement [Patel *et al.*, J. Chem. Phys. **119**, 909 (2003)] that one of these surfaces supports no bound states, and it yields predictions for 27 allowed pure rotational transitions among the truly bound states of the homonuclear isotopologues of this complex. © *2009 American Institute of Physics*.
[DOI: 10.1063/1.3157776]

I. INTRODUCTION

The isoelectronic N_2–He and CO–He systems are prototype many-electron atom-molecule interactions, as they are among the simplest nonhydrogenic van der Waals complexes. The availability of well-resolved infrared (IR) and microwave (MW) van der Waals spectral data has contributed significantly to the development of highly accurate two-dimensional (2D) and three-dimensional potential energy surfaces (PESs) for the CO–He system.[1–3] However, determination of highly accurate 2D and three-dimensional PESs for the N_2–He interaction has proven to be more challenging due to the absence of such spectroscopic data. Nevertheless, a number of PESs have been proposed for the N_2–He interaction over the past 25 yrs, some obtained empirically by fitting proposed functional forms to (nonspectroscopic) experimental data,[4–6] some obtained using semiempirical procedures,[7,8] and some obtained from *ab initio* calculations.[9–13]

Dham and co-workers[8,14] and Stoecklin *et al.*[13] have examined the capabilities of a recent semiempirical exchange-Coulomb (XC) surface[8] and three recent *ab initio* PESs for this system[9,12,13] to provide accurate predictions of cross sections for the molecular beam scattering of He by N_2, and for the temperature dependence of interaction second virial coefficients, of bulk gas transport properties, and of bulk gas relaxation phenomena in N_2–He mixtures. They found that within the experimental uncertainties associated with those data, it is difficult to distinguish clearly between the semiempirical "XC(fit)" PES of Dham *et al.*,[8] the *ab initio* "modified Truhlar expansion" (MTE) PES of Patel *et al.*,[12] and the 2D version of the "BCCD" PES of Stoecklin *et al.*[13] However, they did find that the *ab initio* PES of Hu and Thakkar[9] (HT) yields values for these quantities that often lie outside the experimental uncertainties.

From a "near-side/far-side" analysis[15] of state-to-state differential cross sections as functions of the center-of-mass scattering angle, Stoecklin *et al.*[13] have shown that the available data,[16,17] which span scattering energies of 220–250 cm^{-1}, are only marginally able to distinguish among the semiempirical XC(fit) PES of Ref. 8 and the *ab initio* ("MTE" and BCCD) PESs of Refs. 12 and 13. However, they also showed that analogous measurements at scattering energies of order 10 cm^{-1} (or 1.2 meV) *would* clearly distinguish among them. This result implies that the behaviors of the attractive components of these PESs are sufficiently different that when MW spectra for the N_2–He complex become available, they should provide a clear means of determining which of these surfaces provides a more accurate representation of the N_2–He interaction.

Although no spectra have yet been reported for N_2–He van der Waals complexes, both MW and IR spectra have been observed for the analogous CO–He system:[1,18,19] those data indicate that the CO–He potential supports approximately 13 bound levels. Similarities between the isoelectronic N_2 and CO molecules suggest that the N_2–He interaction should support a similar number of bound levels. Indeed, some evidence for that conclusion has already been provided by the appearance of a glory extremum in the speed dependence of the total integral cross section data of Butz *et al.*,[20] which Candori *et al.*[4] point out as providing evidence for the existence of at least one bound level for this complex. However, given that Patel *et al.*[12] were unable to locate any bound levels for the $^{14,14}N_2$–^{4}He complex on their MTE surface using the TRIATOM program suite of Tennyson *et al.*,[21] it is of interest to examine the ability of the recent N_2–He PESs to support bound states and to predict the MW spectra for the various N_2–He isotopologues.

II. COMPUTATIONAL METHODS

A. PESs

The XC(fit),[8] HT,[9] MTE,[12] and 2D BCCD[11,13] models for the N_2–He system all represent the interaction energy using Jacobi coordinates $V(r,R',\theta')$. As illustrated by Fig. 1, r is the N_2 internuclear separation, which was fixed at the equilibrium bond length of the free molecule, $r_e=2.0743a_0$,[22,23] R' is the length of a vector $\vec{R}'$ from the N_2

[a]Electronic mail: huili@uwaterloo.ca.

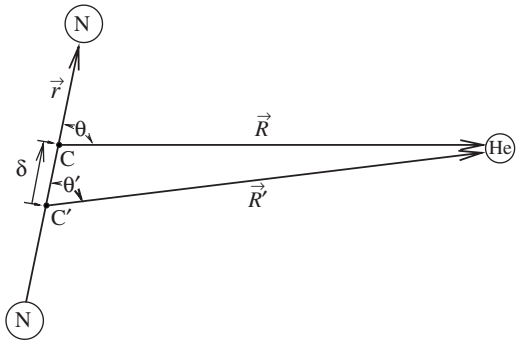

FIG. 1. Jacobi coordinates for N_2–He, where C' and C, respectively, represent the positions of the centers of mass of the homonuclear and heternuclear isotopologues of N_2.

bond midpoint to the He atom, and θ' is the angle between $\vec{R}'$ and the N–N bond vector $\vec{r}$. The fact that the centers-of-mass of the two homonuclear N_2 isotopologues lie at their bond midpoint means that the same intermolecular potential expression may be used when calculating dynamical properties of both $^{14,14}N_2$–He and $^{15,15}N_2$–He. However, although the intermolecular interaction energy is the same for all three N_2 isotopologues (assuming neglect of Born–Oppenheimer breakdown effects), the potential surface used to calculate dynamical properties of He interacting with the heteronuclear $^{14}N^{15}N$ isotopologue differs from that used for the other species due to the noncoincidence of the centers of mass and charge in $^{14}N^{15}N$.

Calculation of dynamical properties of $^{14}N^{15}N$–He requires the $^{14,14}N_2$–He potential energy surface to be subjected to the coordinate transformation shown in Fig. 1. Following the discussion of Refs. 24 and 25, the change in coordinates associated with the shifting of the diatom center-of-mass from C' to C can be expressed through

$$R' = R(1 + t^2 + 2t\cos\theta)^{1/2}, \tag{1}$$

and

$$\cos\theta' = (\cos\theta + t)/(1 + t^2 + 2t\cos)^{1/2}, \tag{2}$$

in which $t \equiv \delta/R$ and δ is the displacement of the center of mass. The intermolecular PES for the nitrogen-helium complex may be expanded as Legendre series in either the new (r,R,θ) or original $(r,R'\theta')$ coordinates

$$\begin{aligned} U(R,\theta) &= \sum_k U_k(R)P_k(\cos\theta) \\ &\equiv V(R',\theta') \\ &= \sum_n V_n(R')P_n(\cos\theta'). \end{aligned} \tag{3}$$

The orthogonality of the Legendre polynomials then allows the expansion functions in the new coordinates $U_k(R)$ to be defined as

$$U_k(R) = \left(k + \frac{1}{2}\right)\int_{-1}^{1} P_k(\cos\theta)V(R',\theta')d(\cos\theta), \tag{4}$$

$$= \left(k + \frac{1}{2}\right)\sum_{n=0}^{\infty}\int_{-1}^{1} P_k(x)V_n(R')P_n(x')dx, \tag{5}$$

in which $x \equiv \cos\theta$, $x' \equiv \cos\theta'$, and the $V_n(R')$ functions are the coefficients of a Legendre expansion for $V(R',\theta')$

$$V_n(R') = \left(n + \frac{1}{2}\right)\int_{-1}^{1} P_n(\cos\theta')V(R',\theta')d(\cos\theta'). \tag{6}$$

In the present work, the functions $U_k(R)$ of Eq. (4) and $V_n(R')$ of Eq. (6) have been determined numerically from $V(R',\theta')$ using 16-point Gaussian quadratures.

B. Bound state energy levels

Within the Born–Oppenheimer approximation, the 2D intermolecular rovibrational Hamiltonian for the $^{14,15}N_2$–He complex in Jacobi coordinates with the total angular momentum represented in the body-fixed reference frame can be written as[26–28]

$$\begin{aligned} \hat{H} = &-\frac{\hbar^2}{2\mu}\frac{\partial^2}{\partial R^2} + \left(\frac{\hbar^2}{2\mu R^2} + B\right) \\ &\times\left(\frac{-1}{\sin\theta}\frac{\partial}{\partial\theta}\sin\theta\frac{\partial}{\partial\theta} + \frac{\hat{J}_z^2}{\sin^2\theta}\right) \\ &+ \frac{\hat{J}^2 - 2\hat{J}_z^2}{2\mu R^2} + \frac{\cot\theta}{2\mu R^2}[(\hat{J}_x + i\hat{J}_y) + (\hat{J}_x - i\hat{J}_y)]\hat{J}_z \\ &+ \frac{\hbar}{2\mu R^2}\frac{\partial}{\partial\theta}[(\hat{J}_x + i\hat{J}_y) - (\hat{J}_x - i\hat{J}_y)] + U(R,\theta), \end{aligned} \tag{7}$$

in which $\mu^{-1} = m_{He}^{-1} + (2m_N)^{-1}$, with m_{He} and m_N being the masses of the He and N atoms,[29] respectively, B is the inertial rotational constant for $^{14,15}N_2$ in its vibrational ground state, and $U(R,\theta)$ is the N_2–He PES. For homonuclear N_2 this operator has the same form except that R is replaced by R', θ by θ', and $U(R,\theta)$ by $V(R',\theta')$. In either case, the operators $\hat{J}_x$, $\hat{J}_y$, and $\hat{J}_z$ are the components of the total angular momentum operator $\hat{\mathbf{J}}$ in the body-fixed frame whose z-axis lies along the Jacobi radial vector $\vec{R}$ (or $\vec{R}'$). This Hamiltonian takes account of full vibration-rotation coupling.

A direct-product discrete-variable representation (DVR) grid[30] has been utilized for all rovibrational energy level calculations for the N_2–He complexes, with an 80-point sin-DVR grid range extending from $4.0a_0$ to $20.0a_0$ covering the radial stretching coordinate R, and a 70-point Gauss–Legendre grid covering the domain of the angular variable. The Lanczos[31] algorithm was employed to calculate the rovibrational energy levels by recursive diagonalization of the discretized Hamiltonian matrix. A doubling of the density of DVR points affects the values of the calculated level energies by less than 0.000 01 cm^{-1}, while extension of the outer end of the radial grid from 20 a_0 to 30 a_0 affects the predicted level energies by less than 0.001 cm^{-1}.

TABLE I. Comparison of the geometries and energies of the stationary points on the XC(fit), HT, MTE, and 2D BCCD PESs for N_2–He. Geometries are given as $\{R(\theta'), V_{min}(\theta')\}$ while lengths are in a_0 and energies in cm^{-1}.

			Collinear saddle point		
PES	Method	T-shaped geometry	Geometry	Barrier	Ref.
XC(fit)	Semiempirical	{6.378, −23.08}	{7.464, −16.37}	6.71	8
HT	MP4/aVTZ[a]	{6.475, −20.88}	{7.526, −16.19}	4.69	9
MTE	CCSD(T)/CBS[b]	{6.404, −23.43}	{7.415, −18.64}	4.79	12
BCCD	BCCD/aVTZ[c]	{6.437, −21.73}	{7.497, −16.43}	5.30	11 and 13

[a]Used the aug-cc-pVTZ(aVTZ) basis set omitting *f* Gaussian type functions on the N atom, and with $3s3p2d1f$ bond functions.
[b]Complete basis set limit (CBS) energies estimated by extrapolating the energies calculated using aug-cc-pVDZ and aug-cc-pVTZ basis sets.
[c]aVTZ basis set with $3s3p2d1f$ bond functions.

III. RESULTS AND DISCUSSION

A. Features of the PESs

Contour plots of the XC(fit), BCCD, MTE, and HT surfaces all have the same basic structure (see, e.g., Fig. 1 of Ref. 13). There is a global minimum at a T-shaped geometry corresponding to $\theta=90°$, and saddle points with no local minima at the collinear N–N–He geometries corresponding to $\theta=0°$ or 180°. The positions and energies of the stationary points for these four PESs are summarized in Table I. The radial positions of the various potential minima differ by less than 1.5%. However, the relative well depth differences are a factor of 10 larger than that, and this can be expected to have significant effects on the energies of the bound states of N_2–He van der Waals complexes. This table also shows that the barrier to internal rotation for the XC(fit) surface is significantly higher (by 27%–43%) than those for the other surfaces, but since the zero-point level on every surface lies more that 10 cm^{-1} (1.5–2.0 times the barrier height) above the corresponding barrier maximum, this difference should have a relatively modest effect on the patterns of level energies.

The Legendre radial strength functions for these surfaces $V_n(R')$ of Eq. (3) for $n=0,2,4,6$ are presented in Fig. 2. Bulk gas properties such as the second virial coefficient and transport coefficients, as well as elastic scattering, depend mainly on the isotropic part of the potential, $V_0(R)$, with only minor effects being due to potential anisotropies ($V_n(R')$ for $n>0$). As shown in Fig. 2, the isotropic radial strength functions $V_0(R)$ do not differ very much among the four PESs considered here; this explains why calculated second virial and transport coefficients for N_2–He mixtures do not differ significantly among these potentials.[8,13,14]

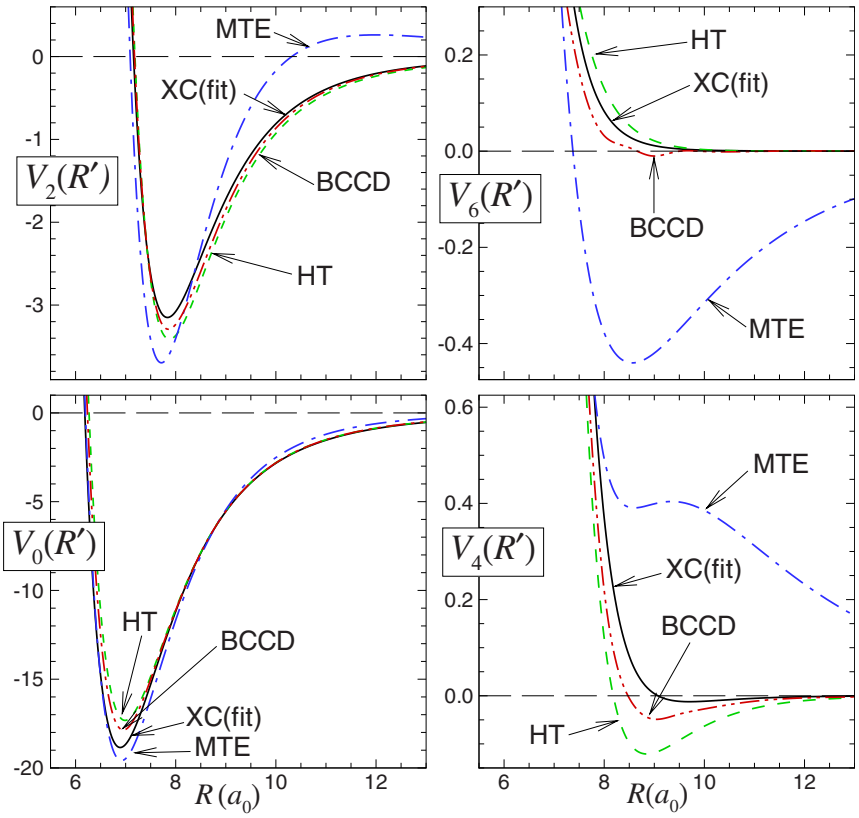

FIG. 2. (Color online) $V_n(R')$ components of the XC(fit), BCCD, MTE, and HT potentials for N_2–He in cm^{-1}.

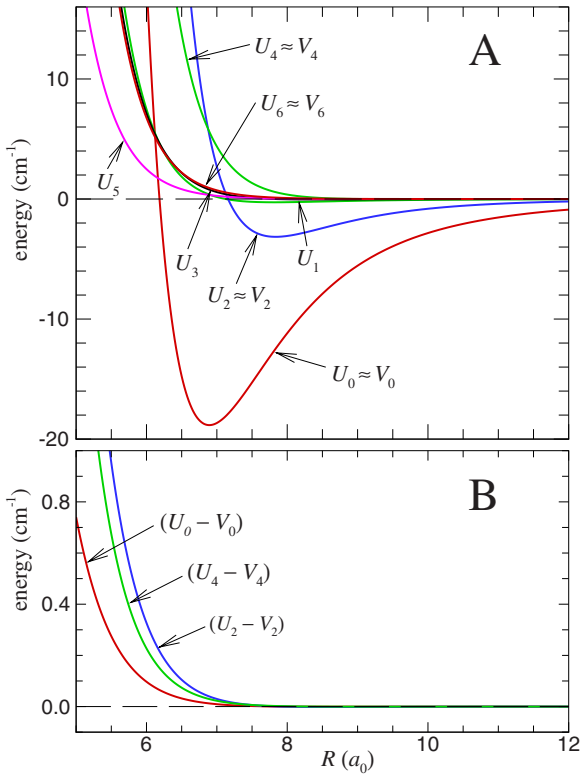

FIG. 3. (Color online) $U_k(R)$ components of the XC(fit) potential for $^{14}N^{15}N-He$.

In contrast with the above, since relaxation phenomena do not occur for isotropic intermolecular interactions, they are particularly sensitive to the anisotropy of a PES. As seen in Fig. 2, the XC(fit), BCCD, and HT potentials yield fairly similar estimates of the leading anisotropic Legendre function, $V_2(R')$; only for the MTE potential does this component shows significant deviations from the others. The right-hand panels of Fig. 2 show that while the behaviors of the second and third anisotropic Legendre radial strength functions $V_4(R')$ and $V_6(R')$ are at least qualitatively similar for three of these surfaces, the components of the MTE potential show markedly different behavior. However, results presented in Ref. 14 show that these large differences in the higher-order anisotropy strength functions do not affect typical relaxation phenomena such as rotational relaxation, collision-broadening of the depolarized Rayleigh light scattering spectrum, or magnetic field-effect phenomena, relative to the (relatively large) experimental uncertainties associated with their experimental determination. This observation is also consistent with the more traditional observation that relaxation phenomena are most sensitive to anisotropy in the radial position of the potential well, positions that do not differ by more than 1.5% for the four PESs under consideration.

Finally, the upper panel of Fig. 3 presents the radial strength functions $U_k(R)$ for $^{14,15}N_2-He$ obtained by applying the transformation discussed in Sec. II A to the XC(fit) potential of Ref. 8. The anisotropy strength functions corresponding to odd values of k arise because of the displacement of the N_2 center of mass from the bond midpoint. The lower panel of Fig. 3 shows that this transformation introduces small (but not negligible) changes to the even-Legendre radial strength functions.

B. Bound states and predicted MW spectrum

Because the anisotropy of the N_2-He PES is relatively weak, it is convenient to label the rovibrational energy levels using the four "space-fixed" coordinate quantum numbers j, l, J, and n_s: j is associated with the rotation of a free N_2 molecule, l with the rotation of the N_2-He axis (i.e., of $\vec{R}'$ or $\vec{R}$), J is the total rotational angular momentum quantum number for the complex ($\vec{J}=\vec{j}+\vec{l}$), and n_s is the quantum number associated with stretching of the van der Waals coordinate R. If the anisotropy were sufficiently strong, it would be more appropriate to use a body-fixed coordinate description and to replace l with K and j with a bending quantum number n_b. However, in the present case the zero-point level lies far above the barrier to internal rotation, and the space-fixed quantum numbers provide a more useful set of labels. Note, however, that J is the only "exact" quantum number, and that (j,l,n_s) are merely convenient sets of labels for identifying a particular level. Of course, in the absence of potential anisotropy, the energy levels corresponding to a set of J-values obtained from a particular (j,l)-pair would be degenerate.[32] All level energies and wave functions reported herein were obtained using the 2D DVR method and the Lanczos propagation algorithm described in Sec. II B.

Table II lists the energies of all bound rovibrational energy levels of the three N_2 isotopologues of N_2-^4He obtained from the XC(fit), BCCD, MTE, and HT potentials, as well as those for $^{14,14}N_2-^3He$ on the XC(fit) PES. As shown there, each PES supports only two $J=0$, bound states of the N_2-^4He complex, and none of the surfaces considered supports any $n_s=1$ excited van der Waals stretch levels. Even the $(j,l,J)=(0,0,0)$, ground state of the $^{14}N_2-^4He$ complex is rather weakly bound; for the XC(fit) PES it lies at -6.8172 cm^{-1} and the first excited $J=0$, state lies at -1.2390 cm^{-1}; similar values are associated with the other PESs.

The nodal structures of the wave functions for three representative levels of the XC(fit) surface are shown in Fig. 4. The wave functions for the four other levels labeled by $j=0$, have qualitatively the same pattern as that for the $(j,l,J)=(0,0,0)$, state shown in the uppermost panel of this figure. Similarly, the wave functions of all levels labeled by $j=1$, have either the nodal pattern seen in the middle panel, when $l \neq J$, or that in the lowest panel, when $l=J$. These nodal patterns clearly confirm the appropriateness of using space-fixed quantum number labels for these states.

For the XC(fit) potential, Fig. 5 shows the positions of the truly bound levels of $^{14,14}N_2-^4He$ relative to the isotropic potentials dissociating to $N_2(j=0)$ and $N_2(j=1)$. The energies labeled by values of l are the energy levels obtained upon ignoring the potential anisotropy, while those labeled with the total angular momentum quantum number J are the actual eigenvalues for the full potential. For the homonuclear N_2 isotopologues, the six levels associated with $j=1$ that lie between the asymptotes for dissociation to $N_2(j=0)$ and $N_2(j=1)$ are truly bound, because the absence of odd-order potential anisotropy means that they are not coupled to the open $j=0$ channels, which would yield $j=0$ N_2 fragments.

TABLE II. Energy levels (in cm^{-1}) of N_2–^{4}He van der Waals complexes, relative to the asymptote for dissociation to He+$N_2(j=0)$. Energies in parentheses are for levels which are metastable with respect to predissociation by internal rotation.

	$^{14,14}N_2$–^{4}He				$^{15,15}N_2$–^{4}He				$^{14,15}N_2$–^{4}He				$^{14,14}N_2$–^{3}He
(l,J)	XC(fit)	HT	MTE	BCCD	XC(fit)	HT	MTE	BCCD	XC(fit)	HT	MTE	BCCD	XC(fit)
			$j=0$				$j=0$				$j=0$		$j=0$
(0,0)	−6.817	−5.889	−7.055	−6.213	−6.875	−5.939	−7.112	−6.265	−6.846	−5.914	−7.084	−6.240	−5.586
(1,1)	−6.229	−5.327	−6.464	−5.641	−6.289	−5.379	−6.525	−5.697	−6.259	−5.353	−6.495	−5.669	−4.869
(2,2)	−5.064	−4.215	−5.294	−4.511	−5.132	−4.274	−5.362	−4.573	−5.098	−4.245	−5.328	−4.542	−3.460
(3,3)	−3.353	−2.587	−3.570	−2.852	−3.429	−2.654	−3.648	−2.922	−3.392	−2.621	−3.610	−2.888	−1.421
(4,4)	−1.150	−0.503	−1.340	−0.519	−1.236	−0.579	−1.429	−0.804	−1.193	−0.542	−1.385	−0.765	⋯
			$j=1$				$j=1$				$j=1$		$j=1$
(0,1)	−3.032	−2.030	−3.244	−2.381	−3.348	−2.341	−3.561	−5.697	−3.190	−2.186	−3.402	−2.537	−1.742
(1,1)	−2.757	−1.718	−2.953	−2.083	−3.076	−2.029	−3.272	−2.399	−2.917	−1.873	−3.113	−2.241	−1.341
(1,2)	−2.264	−1.344	−2.490	−1.664	−2.584	−1.658	−2.811	−1.980	−2.424	−1.501	−2.651	−1.822	−0.868
(1,0)	−1.239	−0.683	−1.546	−0.870	−1.554	−0.991	−1.863	−1.181	−1.397	−0.838	−1.705	−1.026	−0.011
(2,2)	−1.543	−0.557	−1.738	−0.904	−1.870	−0.877	−2.066	−1.227	−1.707	−0.717	−1.903	−1.066	0.133
(2,3)	−1.009	−0.179	−1.240	−0.466	−1.336	−0.499	−1.569	−0.789	−1.173	−0.339	−1.405	−0.628	0.607
(2,1)	−0.451	0.126	−0.729	−0.072	−0.771	−0.189	−1.051	−0.388	−0.612	−0.033	−0.891	−0.231	1.003
(3,3)	0.243	1.143	0.051	0.827	−0.094	0.813	−0.287	0.495	(0.074)	(0.978)	−0.119	(0.660)	2.269
(3,4)	0.737	1.462	0.514	1.353	0.400	1.134	0.176	0.881	(0.568)	(1.297)	(0.345)	(1.046)	2.654
(3,2)	1.005	1.571	0.772	1.376	0.676	1.247	0.440	1.051	(0.839)	(1.403)	(0.605)	(0.660)	2.792
(4,4)	2.548	3.321	2.366	3.052	2.199	2.981	2.016	2.708	(2.372)	(3.150)	(2.190)	(2.879)	⋯
(4,5)	2.933	3.528	2.740	3.326	2.586	3.191	2.391	2.985	(2.759)	(3.358)	(2.565)	(3.154)	⋯
(4,3)	3.006	3.513	2.835	3.341	2.667	3.180	2.492	3.005	(2.836)	(3.346)	(2.662)	(3.172)	⋯

This means that all four PESs predict the existence of 18 truly bound levels for these species. This contradicts the report in Ref. 12 that their TRIATOM calculations found no bound states for this system.

In contrast with the case for the homonuclear N_2 isotopologues, for $^{14,15}N_2$–^{4}He the six (or five for the MTE potential) levels lying above the $j=0$, asymptote are metastable, since the odd-order anisotropies introduced by the coordinate transformation of Eqs. (1)–(6) do couple them to open $j=0$ dissociation channels. Hence, this species is predicted to have only 12 (13 for the MTE potential) truly bound states. However, those six (or five) metastable levels may be expected to be fairly long-lived, since the fact that neglect of the odd-order anisotropies only shifts the bound-state energies by approximately 0.002 cm^{-1} means that this coupling is fairly weak.[33] Thus, these metastable "Feshbach resonance" levels may still be observable in a spectroscopic experiment.

Finally, Table III compares the 27 MW transition energies among the truly bound levels of $^{14,14}N_2$–^{4}He predicted using the four PESs of interest here. As discussed long ago for the case of H_2-{rare gas} complexes,[34] an isotropic "overlap dipole" gives a $\Delta l=\pm 1$, selection rule for transitions among $j=0$, levels, while a quadrupole-induced dipole gives rise to $\Delta l=\pm 1$ and ± 3 transitions among $j=1$, states, with all transitions being subject to the usual $\Delta J=0, \pm 1$ overall selection rule. Ortho-para transitions with $\Delta j=1$, are forbidden for the homonuclear N_2 species, while all levels for which $j\geq 2$ are metastable and hence unlikely to be readily observed. "Stick spectra" showing the different patterns of the rotational transitions for the four PESs are shown in Fig. 6.

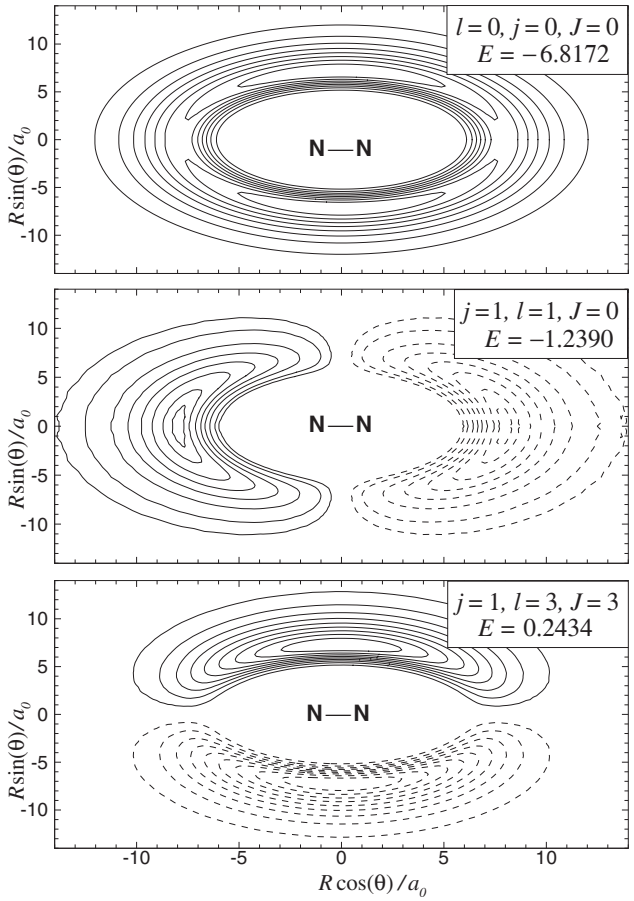

FIG. 4. Wave functions for three representative states of N_2–He. Positive value contours are shown as solid curves and negative contours as dashed curves.

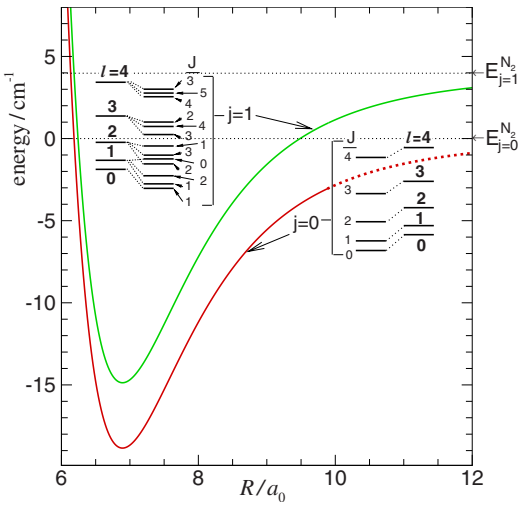

FIG. 5. (Color online) Bound energy levels for the $^{14,14}N_2$–He complex calculated from the XC(fit) potential.

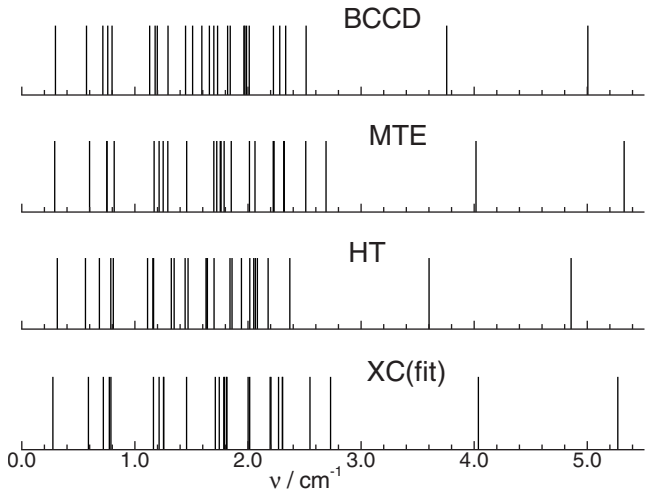

FIG. 6. Predicted MW transitions from Table III.

The predicted MW spectra obtained from all of these surfaces are clearly quite distinct from one other. However, the MTE predictions are much more similar to the others than might be expected in view of the marked differences in the anisotropy strength functions shown in Fig. 2. This probably indicates that the $V_4(R')$ and $V_6(R')$ anisotropy strength functions are too weak to affect the energies of the truly bound levels significantly, and that over the range spanned by the bound-state wave functions, the radial average of the $V_2(R')$ functions for these potentials are very similar, in spite of the different radial behaviors seen in the upper/left-hand panel of Fig. 2. However, the unphysical *positive* long-range behavior of $V_2(R')$ for the MTE potential and marked differences between its higher-order anisotropy strength functions and those for the other surfaces leads to the conclusion that it is somewhat unrealistic.

IV. CONCLUSIONS

Four PESs[8,9,11–13] representing the N_2–He interaction energy have been employed recently for the calculation both

TABLE III. Predicted MW transitions among truly bound levels of the four PESs in cm^{-1}.

j	$(l',J')-(l'',J'')$	XC(fit)	HT	MTE	BCCD
0	(1,1)–(0,0)	0.589	0.563	0.599	0.572
	(2,2)–(1,1)	1.164	1.112	1.170	1.131
	(3,3)–(2,2)	1.711	1.629	1.724	1.659
	(4,4)–(3,3)	2.203	2.083	2.230	2.333
1	(1,1)–(0,1)	0.275	0.314	0.291	0.298
	(1,2)–(0,1)	0.774	0.686	0.753	0.717
	(1,0)–(0,1)	1.793	1.347	1.698	1.510
	(2,2)–(1,2)	0.721	0.787	0.752	0.760
	(2,1)–(1,0)	0.788	0.809	0.817	0.798
	(2,2)–(1,1)	1.214	1.159	1.214	1.179
	(2,3)–(1,2)	1.255	1.165	1.250	1.198
	(2,1)–(1,2)	1.813	1.470	1.762	1.592
	(2,1)–(1,1)	2.306	1.841	2.224	2.011
	(3,3)–(2,3)	1.253	1.322	1.291	1.293
	(3,2)–(2,1)	1.457	1.444	1.458	1.448
	(3,4)–(2,3)	1.746	1.641	1.755	1.820
	(3,3)–(2,2)	1.786	1.700	1.789	1.731
	(3,2)–(2,3)	2.015	1.638	2.013	1.843
	(3,2)–(2,2)	2.548	2.016	2.511	2.281
	(4,4)–(3,3)	2.304	2.178	2.316	2.225
	(4,3)–(3,3)	2.730	2.370	2.690	2.514
	(4,4)–(3,4)	1.811	1.859	1.852	1.698
	(4,5)–(3,4)	2.196	2.065	2.226	1.972
	(4,3)–(3,4)	2.270	2.051	2.321	1.987
	(4,3)–(3,2)	2.001	1.942	2.062	1.964
	(3,2)–(0,1)	4.037	3.601	4.016	3.757
	(4,3)–(1,2)	5.270	4.857	5.326	5.005

of microscopic[13,14] (molecular beam scattering) and bulk gas[8,13,14] (second interaction virial, transport, and relaxation coefficients) for comparison with experiment. The bulk properties were compared upon the basis of dimensionless root-mean-square deviation (DRMSD) values. The DRMSD values determined from a total of 170 bulk property measurements were greater than one for all four PESs examined, but differed by less than a factor of two from smallest, for the semiempirical XC(fit) PES,[8] to largest, for the *ab initio* HT PES.[9] Although none of the PESs performed spectacularly well, the XC(fit) PES appears to be slightly superior to the others based upon its smaller DRMSD value for the bulk gas properties, its comparable agreement with the molecular beam scattering data, and the flexibility remaining in its parametrization, which would allow for the accommodation of higher-quality bulk gas relaxation data (such as nuclear magnetic resonance relaxation times), should they become available.

The inability of the experimental data to discriminate clearly between the semiempirical XC(fit) PES and the two *ab initio* N_2–He PESs[11–13] obtained via coupled cluster supermolecule calculations (MTE and BCCD) attests to the high level of accuracy with which an *ab initio* PES now can be determined. As the close similarity of the four PESs has made it difficult to differentiate[9,13,14] clearly and unequivocally among them on the basis of comparisons with virial and bulk transport-relaxation coefficients or with existing molecular beam scattering data,[9,13,14] Stoecklin *et al.*[13] utilized a near-side/far-side scattering analysis to show that state-to-state differential scattering experiments at scattering energies of order 10–20 cm^{-1} would provide clear differentiation among the four PESs.

It has been shown here that an even clearer distinction would be made based through the measurement of the MW spectrum associated with the bound states of the N_2–He van der Waals dimer. The bound-state energies and the allowed MW transition frequencies for the $^{14,14}N-^4He$, $^{15,15}N_2-^4He$, and $^{14,15}N_2-^4He$ isotopologues given in Tables II and III, respectively, clearly indicate that the MW spectrum for the N_2–He dimer would readily distinguish between the four PESs.

[1] C. E. Chuaqui, R. J. Le Roy, and A. R. W. McKellar, J. Chem. Phys. **101**, 39 (1994).
[2] R. J. Le Roy, C. Bissonnette, T. H. Wu, A. K. Dham, and W. J. Meath, Faraday Discuss. **97**, 81 (1994).
[3] A. K. Dham and W. J. Meath, Mol. Phys. **88**, 339 (1996).
[4] R. Candori, F. Pirani, F. Vecchiocattivi, F. A. Gianturco, U. T. Lamanna, and G. Petrella, Chem. Phys. **92**, 345 (1985).
[5] L. Beneventi, P. Casavecchia, and G. G. Volpi, J. Chem. Phys. **85**, 7011 (1986).
[6] F. A. Gianturco, M. Venanzi, R. Candori, F. Pirani, F. Vecchiocattivi, A. S. Dickinson, and M. S. Lee, Chem. Phys. **109**, 417 (1986).
[7] R. R. Fuchs, F. R. W. McCourt, A. J. Thakkar, and F. Grein, J. Phys. Chem. **88**, 2036 (1984).
[8] A. K. Dham, F. R. W. McCourt, and A. S. Dickinson, J. Chem. Phys. **127**, 054302 (2007).
[9] C. H. Hu and A. J. Thakkar, J. Chem. Phys. **104**, 2541 (1996).
[10] J. P. Reid, A. J. Thakkar, P. W. Barnes, E. F. Archibong, H. M. Quiney, and C. J. S. M. Simpson, J. Chem. Phys. **107**, 2329 (1997).
[11] T. Stoecklin, A. Veronin, and J. C. Rayez, Phys. Rev. A **66**, 042703 (2002).
[12] K. Patel, P. R. Butler, A. M. Ellis, and M. D. Wheeler, J. Chem. Phys. **119**, 909 (2003).
[13] T. Stoecklin, A. Voronin, A. K. Dham, J. Sanchez-Fortún Stoker, and F. R. W. McCourt, Mol. Phys. **106**, 75 (2008).
[14] J. Sanchez-Fortún Stoker, A. K. Dham, F. R. W. McCourt, and A. S. Dickinson, J. Chem. Phys. **128**, 214309 (2008).
[15] P. McCabe, J. N. L. Connor, and D. Sokolovski, J. Chem. Phys. **108**, 5695 (1998).
[16] M. Faubel, K. H. Kohl, J. P. Toennies, K. T. Tang, and Y. Y. Yung, Faraday Discuss. Chem. Soc. **73**, 205 (1982).
[17] M. Faubel, in *Status and Future Developments in the Study of Transport Properties*, NATO ASI Series C: Mathematical and Physical Sciences, edited by W. A. Wakeham, A. S. Dickinson, F. R. W. McCourt, and V. Vesovic (Kluwer, Dordrecht, 1992), Chap. 4, pp. 73–115.
[18] M.-C. Chan and A. R. W. McKellar, J. Chem. Phys. **105**, 7910 (1996).
[19] A. R. W. McKellar, Y. Xu, W. Jäger, and C. Bissonnette, J. Chem. Phys. **110**, 10766 (1999).
[20] H. P. Butz, R. Feltgen, H. Pauly, and H. Vehmeyer, Z. Phys. **247**, 70 (1971).
[21] J. Tennyson, S. Miller, and C. R. Le Sueur, Comput. Phys. Commun. **75**, 339 (1993).
[22] K. P. Huber and G. Herzberg, *Constants of Diatomic Molecules* (Van Nostrand Reinhold, New York, 1979).
[23] R. J. Le Roy, Y. Huang, and C. Jary, J. Chem. Phys. **125**, 164310 (2006).
[24] H. Kreek and R. J. Le Roy, J. Chem. Phys. **63**, 338 (1975).
[25] W. K. Liu, J. E. Grabenstetter, R. J. Le Roy, and F. R. McCourt, J. Chem. Phys. **68**, 5028 (1978).
[26] B. R. Johnson and W. P. Reinhardt, J. Chem. Phys. **85**, 4538 (1986).
[27] S. E. Choi and J. C. Light, J. Chem. Phys. **92**, 2129 (1990).
[28] B. T. Sutcliffe and J. Tennyson, Int. J. Quantum Chem. **39**, 183 (1991).
[29] G. Audi, A. H. Wapstra, and C. Thibault, Nucl. Phys. A **729**, 337 (2003).
[30] J. C. Light, I. P. Hamilton, and J. V. Lill, J. Chem. Phys. **82**, 1400 (1985).
[31] C. Lanczos, J. Res. Natl. Bur. Stand. **45**, 255 (1950).
[32] R. J. Le Roy and J. van Kranendonk, J. Chem. Phys. **61**, 4750 (1974).
[33] R. J. Le Roy, M. R. Davies, and M. E. Lam, J. Phys. Chem. **95**, 2167 (1991).
[34] A. R. W. McKellar and H. L. Welsh, J. Chem. Phys. **55**, 595 (1971).